Design of Rigid-Flex PCB Robotics Leveraging Validated Finite Element Simulations

John Bell
Clemson University
Glenn Department of Civil Engineering
S Palmetto Blvd
Clemson, SC 29634
jsb6@clemson.edu

Dr. Laura Redmond
Clemson University
JPL-affiliate
Glenn Department of Civil Engineering
Department of Mechanical Engineering
S Palmetto Blvd
Clemson, SC 29634
NASA Jet Propulsion Laboratory
California Institute of Technology
4800 Oak Grove Dr., Pasadena, CA, 91109
lmredmo@clemson.edu

Kalind Carpenter
Robotic Vehicles and Manipulators Group
NASA Jet Propulsion Laboratory
California Institute of Technology
4800 Oak Grove Dr
Pasadena, CA 91109
kalind.c.carpenter@jpl.nasa.gov

Dr. Jean-Pierre de la Croix
Maritime and Multi-Agent Autonomy
NASA Jet Propulsion Laboratory
California Institute of Technology
4800 Oak Grove Dr
Pasadena, CA 91109
Jean-Pierre.de.la.Croix@jpl.nasa.gov

Abstract— **The use of rigid-flex printed circuit board (PCB) as primary structure has the potential to reduce the weight and volume of robotic systems. In the case of robotics for interplanetary exploration, these systems can leverage origami-inspired folding for increased mobility options and reduced storage volume. Folding rigid-flex PCB robotics can be constructed with rigid PCB connected by short Nomex fabric hinges coupled with flex PCB ribbon cables that permits enhanced system flexibility and energy dissipation to promote impact survivability. This paper presents a design methodology of rigid-flex PCB systems with an emphasis on impact resistance. The design process considers solder joint adequacy, panel bending, and fracture using a finite element (FE) model. The proposed design methodology is developed using a case study with NASA JPL's Pop-Up Folding Flat Explorer Robot (PUFFER). First, the finite-element (FE) modeling methodology is presented with consideration to both frequency and time-domain modeling applications, which include operational self-contact analysis and high impact scenarios. The time-domain impact modeling methodology utilizes hyperelastic material properties for the Nomex hinges. This modeling method is validated using image correlation of PUFFER drop tests. A flowchart is presented to guide users through a validated Abaqus modeling procedure for highly flexible rigid-flex systems. Next, a case study is presented in which PUFFER is subject to drop heights representative of falls into Lunar pits and then the design is refined for a more optimum impact performance. Finally, the results of the case study are used to inform a generalized design methodology for rigid-flex PCB robotics subject to high-impact loads with the considerations presented.**

TABLE OF CONTENTS

978-1-6654-3760-8/22/$31.00 ©2022 IEEE

1. INTRODUCTION

Rigid-flex printed circuit board (PCB) assemblies are the combination of standard, rigid PCB panels combined with flexible hinge-type elements. In some cases, the flexible component is flat cabling connecting the mounted components on adjacent panels. In others, the flexible component is reinforced by a compliant material that spans the gap. Rigid-flex PCBs bring novel improvements to robotic design and and can be used to construct origami-type robots created for space exploration settings. These robots can leverage the folding mechanisms for mass and volume optimization, and the addition of degrees of freedom to these systems allows for collapse and dissipate energy through the compliant material.

When designing rigid-flex PCB robotics for dynamic environments, unique challenges beyond the kinematics of the system merit sophisticated models to understand their behavior. Established methods for origami design [1, 2] and estimated mass/inertial properties can be used in the preliminary design stages. However, no current methodology exists to virtually iterate on the design of rigid-flex PCB robotics that considers complexities such as: panel distortions due to local impact forces, dynamics during launch/landing sequences, and panel-to-panel contact under high loads.

To aid in the design of rigid-flex robotics this paper will provide a high-level overview of a validated finite element (FE) modeling approach utilizing NASA JPL's Pop-Up Folding Flat Explorer Robot (PUFFER) [3] as a case study with special consideration to dynamic loading. PUFFER's hinges are constructed from thin strips of a fiber-based fabric, Nomex® [4], in addition to preexisting cabling. A Nomex joint connecting two rigid PCB panels is shown in Figure

1. The proposed FE approach is validated with modal and impact testing in both the time and frequency domains for both implicit and explicit solver environments. Next, a case study of dynamic impact performance of PUFFER is used to illustrate some of the design principles for rigid-flex PCB robotics. Finally, general design guidance will be provided for rigid-flex PCB systems leveraging the validated FE approach. These general guidelines will be demonstrated through a series of benchmark models.

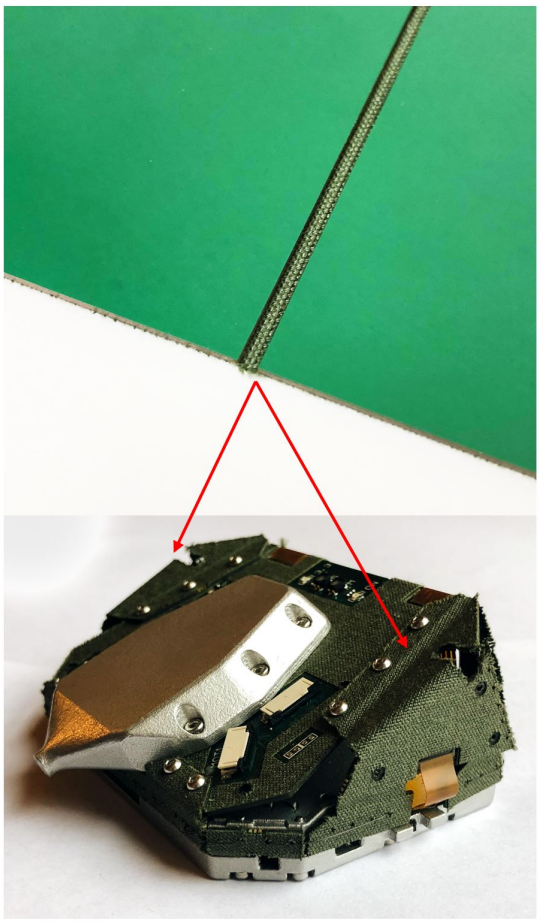

Figure 1. Thin Nomex hinge (1.693 mm) bridging two rigid PCB panels (top) and two example joint locations shown on PUFFER's chassis (bottom)

2. Modeling Methodology

The FE modeling methodology proposed is satisfactory for and has been validated to accurately capture dynamic behavior in both frequency and time-domain settings. A brief description of each modeling method is provided as the method of modeling the Nomex hinge behavior varies for each domain. Two different time-domain methods will be discussed: an implicit time domain methodology suitable for launch and operational dynamic analysis (small-deformation) and an explicit time domain methodology suitable for large-displacement impact analysis. These will be presented using PUFFER as the case study structure. A flowchart outlining the modeling methodology (Figure 5) is presented following the discussion of the three modeling procedures.

The PUFFER chassis model is shown in Figure 2. For model simplification, the wheels and antenna attached [3] are not included in the model and may be represented as lumped mass and inertial elements. This model leverages shell elements for the rigid panels, solid elements for the aluminum base and top cover, and rigid elements for local stiffening of mounted electronic components. Units are expressed in kN, GPa, mm, and ms, and the mesh size is set to a maximum of 1mm. All panels have contact definitions applied and point masses for the larger components were added in the respective locations. The total mass of the chassis is 0.151 kg and has dimensions of 92 mm x 57 mm x 34 mm.

Bending of PCB panels under various dynamic loads and boundary conditions is a well-researched topic [5–8]. PCB panels are laminated composites with both insulating and conductive layers. These are often represented as an isotropic material through it's thickness. This assumption dramatically reduces FE complexity by permitting 2D elements to represent the panels. Arabi et al. [9] computes a effective elastic modulus and density for a given PCB layup. Bell et al. [10] utilizes this approach, but more sophisticated rigid PCB material models could be implemented.

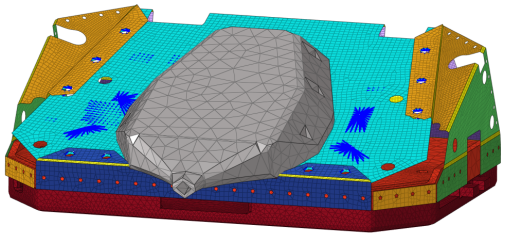

Figure 2. PUFFER chassis FEM

Frequency Domain

Modeling rigid-flex PCB structures to accurately capture dynamics utilizes a "modified plate hinge" method presented in [10]. This method modifies the equations for axial and bending rigidities, A_r and B_r, respectively,

$$B_r = \frac{Et^2}{12(1-\nu)} \tag{1}$$

$$A_r = \frac{Et}{1-\nu^2} \tag{2}$$

where E is Young's modulus, t is the plate thickness, and ν is Poisson's ratio.

A modification of E, t, and the plate element material density, ρ, allow for the adjustment of the bending rigidity while retaining similar axial rigidity properties. This methodology is discussed in detail in [10]. This methodology coupled with a high-fidelity, finely-meshed model yields satisfactory frequency-domain results, but is unsatisfactory for the large-deformation dynamic results shown in this paper.

Implicit Time Domain

For models capturing the response of a rigid-flex structure at relatively low deflection levels or subject to various vibration profiles, it is best to utilize Abaqus' implicit (standard) solver. The time-domain model necessitated a different form of construction than the frequency-domain model because of artificial stresses that can be carried by the Nomex plate element joints upon system bending and folding as shown in Figure 3.

To retain model simplicity and avoid any implementation of a two-step pre- and post-buckling model with an imperfection

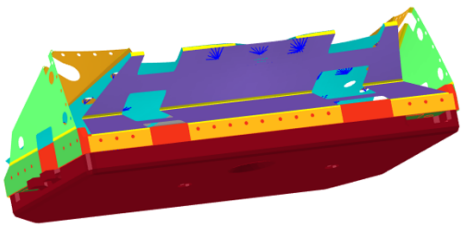

Figure 3. PUFFER chassis FEM

in the plate elements, zero-length bushing elements [11] are added to either side of the Nomex plate elements as shown in Figure 4. The implementation of bushing elements provides tailorable axial and rotational stiffness at a single point that can be tuned to match the stiffness observed in testing. This study found that neglecting rotational stiffness did not lead to adequate model results when comparing model deformed shapes to test observations. Additionally, some compression capacity is necessary for model stability and to be representative of a real-world rigid-flex system.

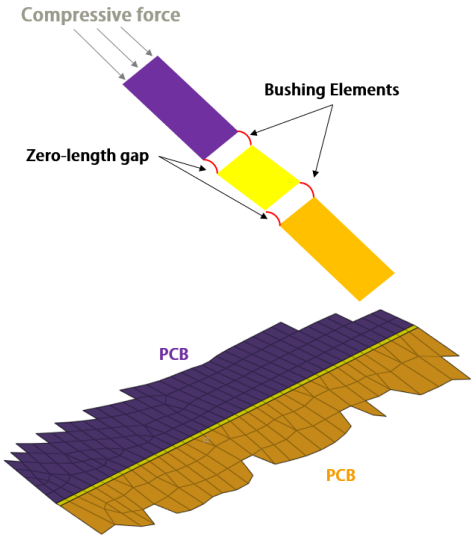

Figure 4. Bushing element hinge FEM construction

A reduction in the rotational stiffness between the PCB and Nomex plate elements allows for the deformation to manifest at the bushing elements instead of forcing the plate elements to buckle, removing a large majority (up to 65%) of the compressive stresses in the Nomex plate elements. Some compression capacity is necessary for model stability and to be representative of a real-world rigid-flex system.

Explicit Time Domain

The explicit solver in Abaqus is often used for high-deformation, contact, or impact problems [12–14]. For impact studies of rigid-flex PCB robotics, this solving environment is recommended. Akin to the transition between the frequency and implicit time-domain spaces, the Nomex plate elements paired with bushing elements will develop artificially high compressive forces for very large deformations or instances where high impact velocities over short time periods do not always allow for compressive forces across a hinge to move off-axis and allow the structure to fold, even with the addition of the bushing elements. Thus an anisotropic-elastic material model was used for the Nomex plate elements to permit softer compression than tension behavior at the hinge plate elements. Applicable to 2D elements in Abaqus Explicit, the Ogden model of hyperelasticity was applied to the explicit time domain models, but adds significant computational expense.

Flowchart

3. Model Validation

The model constructed using the described modeling procedures is validated in both the frequency and time domains.

Frequency Domain

Validation in the frequency domain starts with the validation of the modified plate-hinge model. The validation for this methodology is presented in [10]. A modal test of the entire PUFFER chassis was also conducted over a frequency range from 0 to 4500 Hz in a configuration where the dynamic response PUFFER could be considered approximately linear, as shown in Figure 6. The proposed model was able to capture the first 4 modes of the system within 6.17% of the experimentally determined frequencies and exhibited congruence between FEM and test data mode shapes.

Time Domain

Validation in the time domain and the explicit modeling methodology is performed by drop testing PUFFER's chassis. PUFFER is released from rest at a specified drop height and impacted with the with an angled metal bracket attached to a massive base. In all cases, it is ensured that the base is relatively massive compared to the test specimen to avoid any dissipated energy through the base shifting upon impact.

The drop test heights between 0.30 m and 1.37 m were selected from applying factors of safety to preliminary model results to keep the testing nondestructive. For image correlation, a Photon Mini UX100 camera is used with a f1.8 50mm Nikon lens.A second wide-angle camera was placed with a perpendicular angle to verify proper translational and angular velocities at the time of impact. All drop tests were filmed with 600 frames-per-second (fps). Brightly colored points visually juxtaposed with a black dot in the center were placed on PUFFER to be used for image tracking with a possible error of $\pm$ 0.50 mm. Tracking is performed using the Photron Fastcam Analysis software package by extracting displacement data (Figure 7). It is manually verified for all cases that the algorithmic tracking is operating correctly.

Drop testing is performed by releasing PUFFER from rest at a specific angle to obtain a final desired translational and angular velocity at the moment prior to impact. Many tests were attempted and the best four for image correlation were selected from the results based on shadows, shading, and impact orientation.

As only a single high-speed camera was available 2D camera data was correlated with the model in a fixed frame of reference representing the camera angle; however, this approach should be used with caution. For a displacement vector in $\mathbf{R}^3$ projected onto a plane in $\mathbf{R}^2$, the maximum error (displacement not captured in the projection) is the magnitude of the vector normal to the plane. Several checks were performed to ensure that out-of-plane displacement was not being lost in the transformation.

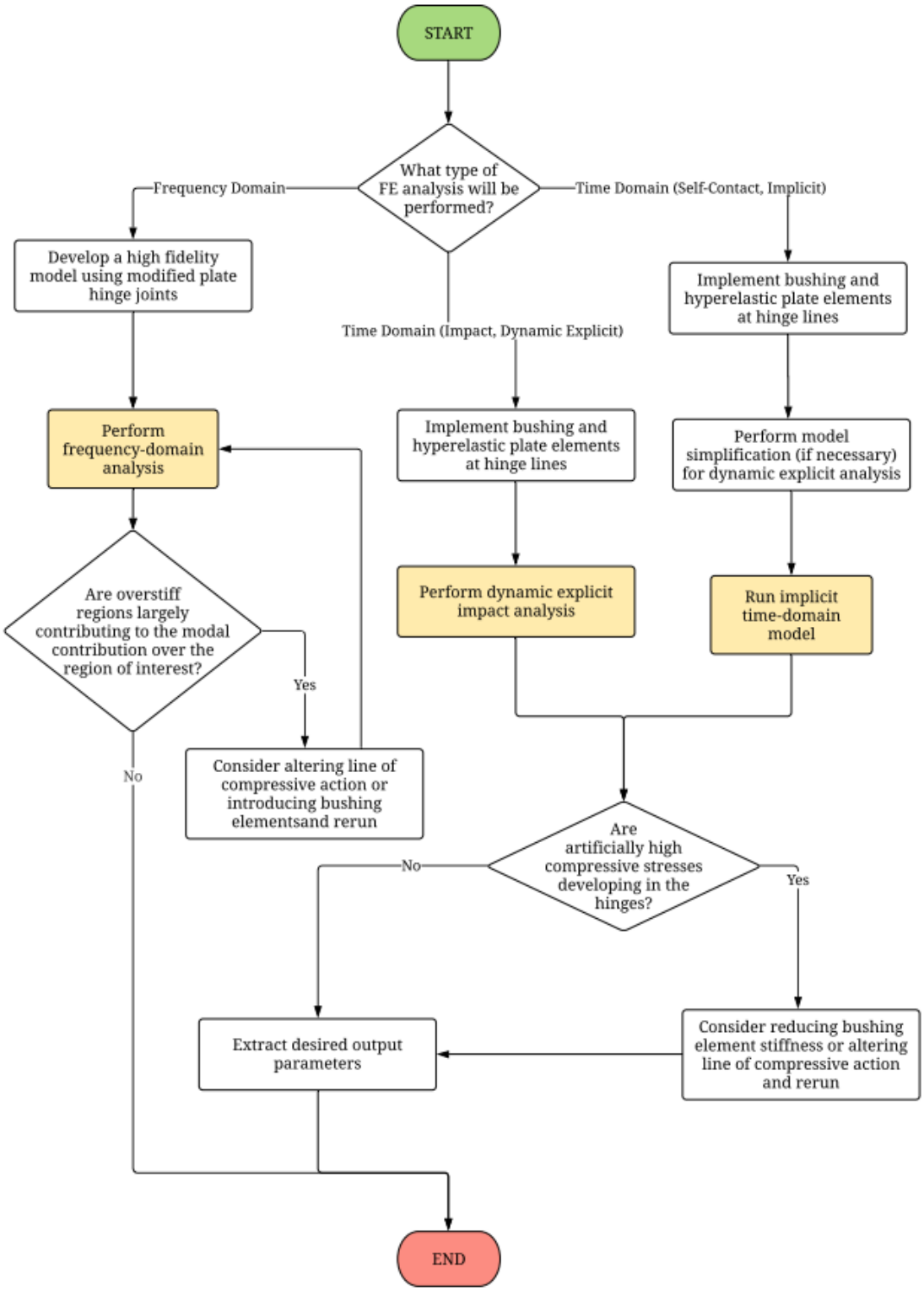

Figure 5. Modeling methodology flowchart for frequency, explicit time domain, and implicit time domain environments

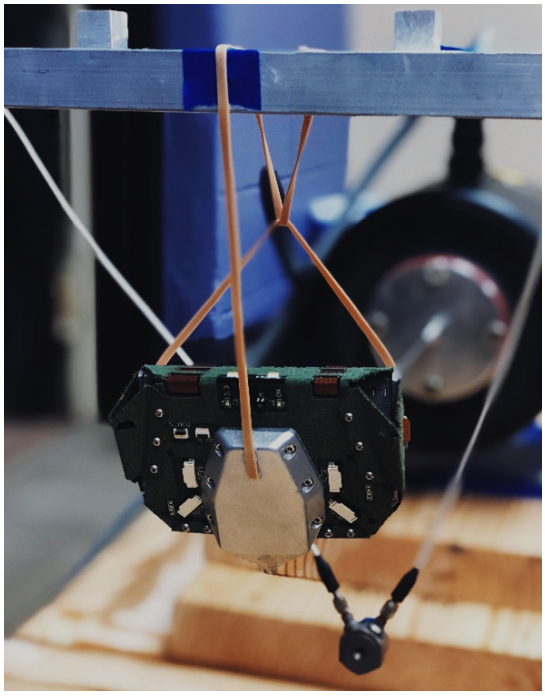

Figure 6. Modal test configuration for PUFFER chassis

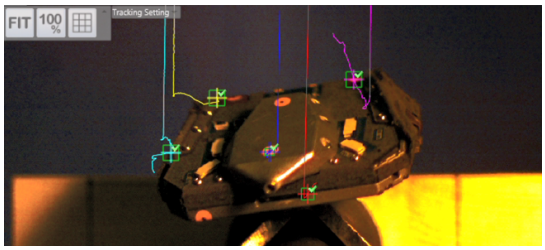

Figure 7. Displacement tracking algorithm on PUFFER's chassis

4. Rigid-Flex PCB Structural Requirements

This section covers the structural considerations taken when implementing a rigid-flex PCB as the primary structural component of a robotic system. These requirements guide the proposed design principles for rigid flex PCB and will be used to assess PUFFER's performance in the impact study and the performance of the proposed alternate origami configurations. For the purposes of structural design for rigid-flex robotics, this paper considers the mechanical failures of a bending stress and fatigue limit states. Attention is drawn to solder joint reliability, but this is highly case-specific and often requires additional studies based on the solder fill material and soldering process implemented. For PUFFER, fracture stresses are not a controlling failure mode, but a high-level discussion is presented for other applications which may have brittle components.

Panel Bending

The rigid components of a rigid-flex system will exhibit bending, even to a small degree, in all operational and impact scenarios. A recommendation from the Jet Propulsion Laboratory for the specific PCB layup used in PUFFER has a typical controlling ultimate stress for PCB based on Arlon (high temperature) 85N polyimide as 120 MPa. This is the value against which bending stresses will be checked for the PUFFER impact study and the additional architectures.

A typical PCB may also be considered a thin plate, which provides multiple options for analytical solutions. For example, if a maximum angle of curvature is determined by sensitive mounted electronic components or conductive pathways, Kirchoff's thin plate theory [15] may be applied. Preliminary hand calculations assessing exposed PCB feasibility is an initial assessment of the stresses encountered in the plate given a robotic structure mass and acceleration.

Fatigue Limit States

Steinberg [5] presents the following equation for a maximum 3σ normal displacement of a PCB panel in bending with a mounted component.

$$Z_{3\sigma} = \frac{0.00022B}{Chr\sqrt{L}} \tag{3}$$

All dimension units in the equation are inches. B is the length of the PCB edge parallel to the component, L is the length of the electronic component, h is the thickness of the PCB,and r and C are factors and constants presented by Steinberg that varies depending on the location and type of electronic component, presented in Tables 1 and 2. For PCB systems that operate with deflections $\leq Z_{3\sigma}$, one would expect the fatigue life to meet 20 million stress reversals. A one-time exceedance of this value does not indicate failure, but design should be such that in operational use the fatigue life of all components of a rigid-flex system should reach 20 million cycles.

Table 1. Position factors for mounted components, *r*

Component location	*r*
Center of the PCB (1/2 x and y)	1.0
Center & quarter of the PCB (1/2 x and 1/4 y)	0.707
Quarter of the PCB (1/4 x and y)	0.50

Table 2. Electronic component constant, *C* [5, 17]

Component type	*C*
Axial leaded through hole or surface mounted components, resistors, capacitors, diodes	0.75
Standard dual inline package (DIP)	1.0
DIP with side-brazed lead wires	1.26
Through-hole pin grid array (PGA) with many wires	1.0
Surface-mounted ball grid array (BGA)	1.75
Surface-mounted leadless ceramic chip carrier (LCCC)	2.25

The classic Steinberg fatigue approach is an estimate and several other factors can be considered when performing fatigue calculations. First, the vibration environment acting on a PCB panel may be a non-Gaussian random vibration, invalidating the $Z_{3\sigma}$ value calculated. For rigid-flex systems, the flexibility of the system encourages more rigid-body displacements, and a non-Gaussian vibration profile is not expected to be an issue.Second, the mounted electronic

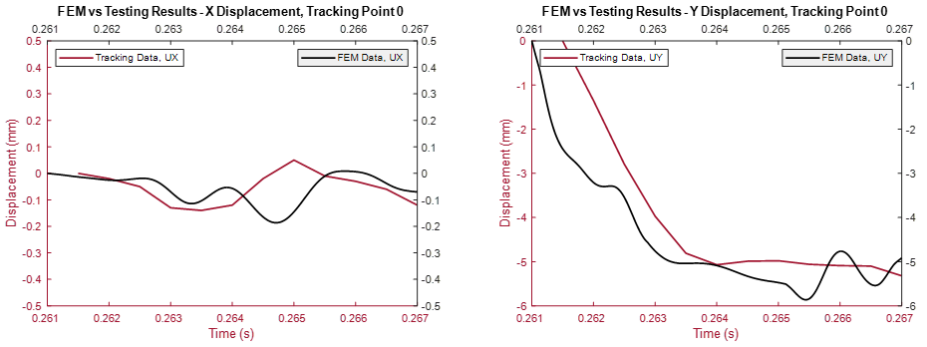

Figure 8. Displacement comparison between drop test and FEM results for tracking point 0

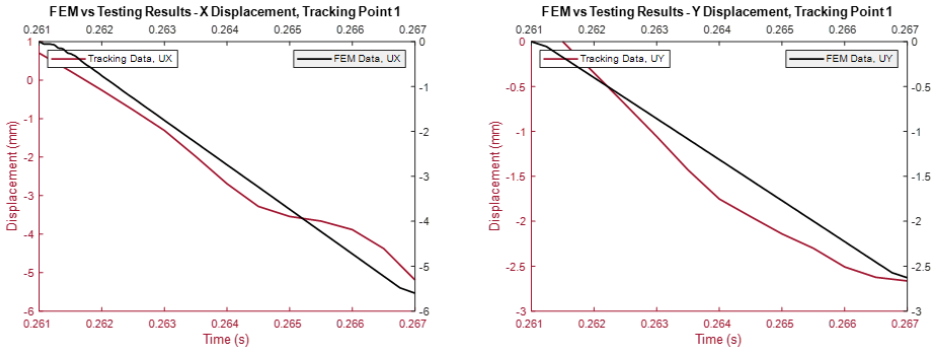

Figure 9. Displacement comparison between drop test and FEM results for tracking point 1

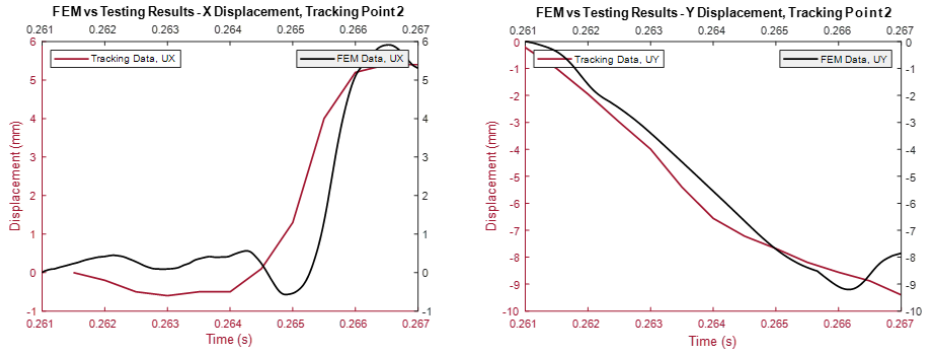

Figure 10. Displacement comparison between drop test and FEM results for tracking point 2

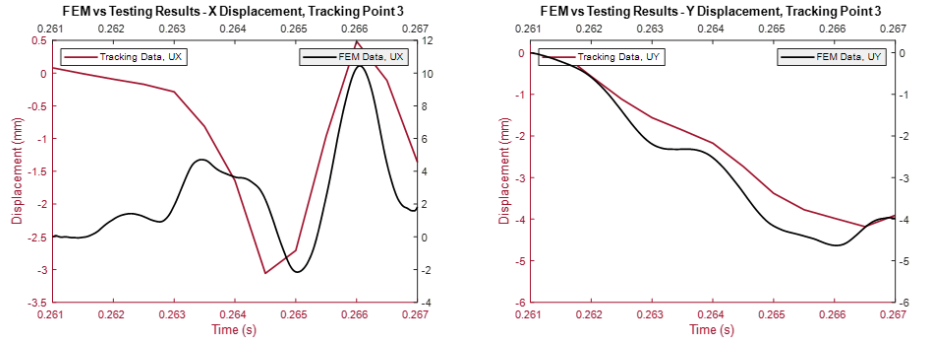

Figure 11. Displacement comparison between drop test and FEM results for tracking point 3

component may be mounted on a panel that responds as a MDOF system with non-negligible bending stresses at higher frequency resonances. It is suggested that if high-frequency resonances are a concern for fatigue, both frequency and time-domain high fidelity models be analyzed. Tom Irvine presents an extension to the Steinberg methodology by taking

into account the maximum relative displacement spectral density curves of PCB panels that are expected from a random vibration input environment [17].

The panels of a rigid-flex system may be assessed individually based on the mounted components, or a more general conservative approach may be taken. For PUFFER, the mounted component providing the minimum value for $Z_{3\sigma}$ in Equation 3 is a surface mounted chip carrier with thermal compression bonded wires with dimensions of 0.79 in x 0.79 in. The corresponding maximum $Z_{3\sigma}$ is 0.331 mm.

The Steinberg fatigue bending criterion is checked upon obtaining Abaqus model results. This is performed by selecting at most four nodes to define a planar PCB or by fractionating a more complex PCB section and defining the subsets by at least four nodes. For the complex U-shaped PCB panel used in PUFFER, three subsections were determined and are shown in Figure 12. This is likely due to large panel unsupported widths (as will be investigated through alternate origami configurations).

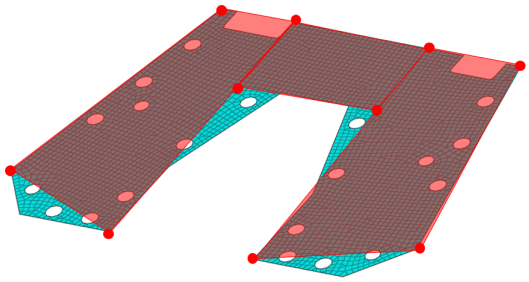

Figure 12. Discretized complex shape PCB panel

Say the boundary nodes are labeled p_1, p_2, p_3, p_4. Nodal coordinates of each node, $coord(p_i) = P_i = [x_i, y_i, z_i]^T$ are extracted at each time step. Depending on mesh size and computation time, either all nodes along the face of the panel may be extracted, or nodes in the center of the discretized sections may be defined. Denote the center nodes as r_1, r_2, r_3, r_4 and the coordinates of these nodes as R_i. At every time step, define a unit vector normal to the plane defined by three boundary nodes:

$$\hat{n} = \frac{(P_1 - P_2) \times (P_1 - P_3)}{||(P_1 - P_2) \times (P_1 - P_3)||} \tag{4}$$

Perform this operation for all combinations of 3 nodes out of the 4 that define the plane. At every time step, calculate a displacement vector for the center node, $\Delta R_i = R_i - R_i^0$. Project this vector onto $\hat{n}$ to extract the normal displacement by computing $\hat{n} \cdot \Delta R_i$. Conservatively select the worst case value out of all combinations of boundary nodes selected.

Solder Joint Reliability

Solder joint adequacy and reliability under dynamic loading is highly sensitive to both solder filler material and the soldering process [18]. Solder joints may experience failure in a high-deformation event by exceeding the tensile strain limit but more often accumulate damage through low or high-level cycles. This vibration-induced fatigue is incredibly difficult to predict due to test conditions, variations in manufacturing, and the anchor point variability [19]. Generally, solder is a flexible and forgiving material, and it is often assumed as adequate [20]. For the purposes of an initial rigid-flex PCB robotic design, it must be ensured that (1) no components with soldered connections are left exposed, and in the event of an impact with a sharp object, the full velocity of the mass and inertia of the robot is transferred into the component and soldered connections and (2) no bending with a relatively tight radius of curvature is occurring at the solder joint locations.

Fracture Stress

A fracture failure relies on the following assumptions: (1) a preexisting imperfection is of the degree that a fracture may propagate and (2) the structure is brittle such that fracture may occur. These assumptions are necessary for the application of Griffith fracture theory [16]. With application to a PCB, the first assumption may be a manufacturing imperfection or a small indentation where the PCB is damaged prior to rigid-flex assembly or in operations prior to an impact event. The second assumption requires an elastic material to fracture in a brittle fashion. In general, the PCB layup of PUFFER is considered to be ductile and fracture is not a significant concern.

If fracture is a concern in the panels, criteria are based on a stress intensity factor K_I [16] and the fracture toughness K_{IC}, a material property. Fracture occurs when $K_I > K_{IC}$. The simplest approach is to conservatively select the lowest fracture toughness value defined by materials in the region of concern. To illustrate a fracture evaluation, we select a fracture toughness for copper to control our design, $K_{IC-cu} = 60MPa/\sqrt{m}$. Griffith fracture theory provides the stress intensity factor for a single-edge crack in a finite width sheet by:

$$K_I = \sigma\sqrt{\pi a} f(\lambda) \tag{5}$$

Where σ is the stress causing fracture, a is the depth of the initial imperfection, $\lambda = a/c$ where c is the width of the panel along the direction of the crack, and $f(\lambda)$ is a value defined in [16]. If a PCB panel has a $\sigma_u = 120MPa$ and is brittle enough to encounter fracture, a plot of the preexisting crack (imperfection) length vs. stress required to propigate the fracture to failure is shown in Figure 13.

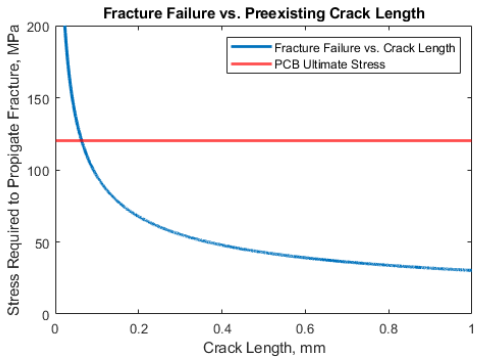

Figure 13. Plot of preexisting crack (imperfection) length vs. the stress required to propigate

We observe that if an imperfection with a length of 0.0795mm or greater is present at the edge of a more brittle PCB panel, any localized ultimate stresses at that point will cause a fracture failure instead of a local yielding failure. This should be a consideration for all brittle materials.

5. PUFFER IMPACT STUDY

To evaluate PUFFER's impact performance on a lunar surface and to outline additional rigid-flex PCB design principles, several FE models with the validated chassis were constructed following the process outlined in Figure 5. The scope of the study is to verify PUFFER's impact survivability against the failure criteria described in the previous section. PUFFER's original design was intended for compact storage and exploring low overhangs on Mars and not explicitly designed for impact events. The prototype was subjected to impact events in order to gain knowledge about the system's potential for impact survivability and help formulate design principles for future rigid-flex PCB robots intended to survive impacts. A worst-case impact scenario encountered by PUFFER on the lunar surface is a drop into a lunar pit with heights up to 80m. These models are conservative by assuming contact with a very sharp point. A lunar gravitational constant is implemented and three primary worst-case impact points were selected through preliminary displacement-controlled models. Lumped masses and rotary inertial elements were added to represent a full operational PUFFER rover. This section will present results from two different impact locations and design adjustments to improve system survivability.

Impact Model Description

Impact models were performed in Abaqus explicit. Two different impact points, both generating significant stresses in the PCB body, are shown in Figure 14. Impact point properties and model information is provided in Table 3.

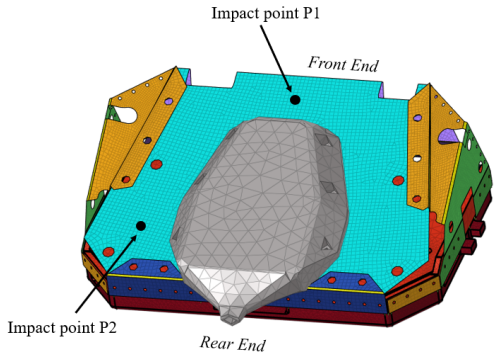

Figure 14. Two presented impact points on PUFFER, P1 and P2

Table 3. PUFFER Impact Model Parameters

Impact Pt.	Drop Height (m)	$V_t \frac{mm}{ms}$	$\omega \frac{rad}{ms}$
P1	40	-11.402	0.087
P2	80	-16.125	0.087

A maximum angular velocity of 0.087 rad/ms is calculated assuming a slow decent off a steep interface, causing contact between the edge and the antenna. All models are 10ms in length and take a minimum of 17 hours to complete. Energy balances were and should be performed with each run completion to ensure adequate results were obtained. For brevity, only one visual set of stress results is shown for impact point P1 at maximum deformation. The elements shown in red are ones that have exceeded the ultimate PCB stress of 120 MPa.

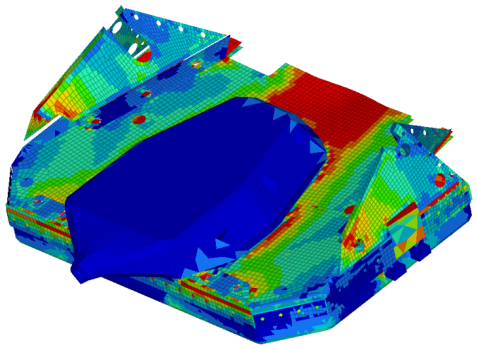

Figure 15. Maximally deformed state of PUFFER at impact point P1 with upper gradient bound set to 120 MPa and masked Nomex joints for clarity

The relevant model results are shown in Table 4. In this table, δ_T is the maximum out of plane deflection, σ^b_{max} is the maximum Von Mises stress due to bending and shear, and σ^c_{max} is the maximum contact force between panels.

Table 4. PUFFER Impact Model Parameters

Impact Pt.	δ_T (mm)	σ^b_{max} (GPa)	σ^c_{max} (GPa)
P1	8.142	2.102	0.446
P2	5.448	0.874	0.2345

PUFFER Design Adjustments

A quick hand calculation verifies that in the event of impact with a sharp rock at an angle close to parallel to the PCB surface, shearing forces in the solder would fail the connection. Thus, the exposed mounted electronics components on PUFFER should be moved internal to the robot or adequate covers provided to improve impact resistance. A second adjustment to the preliminary design is a necessity for the reconfiguration of the attachment of two PCB panels near the rear of the chassis. The existing design calls for two titanium M0 bolts that interfere with the aluminum base at 25° panel closure, generating high bending stresses at the bolt locations. A FEM is created of this phenomenon using nonlinear axial springs to represent the collision between the protruding bolts and the aluminum base. These two high areas of stress can be seen on either side of the antenna in Figure 16.

PCB, acting as the primary structural component of a rigid-flex robot, is the base to which all payloads are attached. Robotic components providing mobility, communication, sensing, e.g., all have mass and inertial characteristics that must be absorbed by the PCB upon impact. PUFFER's preliminay design had the wheels and motors attached to two triangular side panels using titanum bolts and thru-holes. In all impact cases, stress concentrations around these holes near the edge of a PCB panel reached the ultimate stress.

Table 4 outlines the maximum bending and stresses from impact. Both models exhibit a maximum out of plane deformation δ_T that far exceed the calculated Steinberg fatigue criterion of 0.331 mm. The maximum out of plane bending takes place in the center of the U-shaped PCB panel akin to the deformation shown in Figure 15. At 80 and 40 lunar meters, respectively, PUFFER reaches the impact

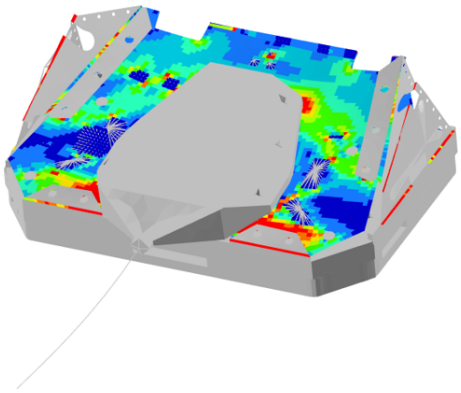

Figure 16. Gradient of stress with red = 120 MPa, identifying problematic connection between adjacent PCB panels

surface with enough velocity to immediately fail the PCB at the given impact point. It is important to interpret this type FEM results with an informed perspective. The model assumes that the PCB is indefinitely linearly elastic, and a physical impact would dissipate energy through some plastic deformation. Additionally, these models assume an impact perfectly normal to the PCB surface which is highly unlikely.

It is valuable to analyze the behavior of rigid-flex systems during impact from an energy perspective. In Abaqus explicit, the following equation for the relevant energy balance parameters is given [21].

$$E_E + E_{CD} + E_A + E_V + E_{FD} + E_{KE} = E_{total} \quad (6)$$

Where E_E is the elastic strain energy, E_{CD} is the energy dissipated by viscoelasticity, E_A is the artificial strain energy, E_V is the viscous energy dissipated, E_{FD} is the frictional energy dissipated, E_{KE} is the kinetic energy, and E_{total} is the total (constant) energy of the system. Design of a rigid-flex PCB robot can take two approaches: a design focusing on maximizing the energy dissipated through kinetic energy or damping and then minimizing the amount of energy contributing to strain and damage in sensitive components.

The model results illustrate the necessity for either a stiffening or protection mechanism for the external PCB panels. A small addition to mission payload through an increase of structural weight outweighs the benefits of having potentially vulnerable PCB surfaces exposed in an impact event. A hand calculation for both scenarios yields that solders at pins at mounted components would fail with the resulting bend radii in the panels. This leads to the recommendation that aluminum plates or a skeleton-type structure be constructed to abut and stiffen the PCB panels in weaker sections. It is also evident that the encountered stresses, even at the edges of the panels where fracture would occur, would easily propagate any preexisting deformities or cracks incurred through operation to the point of impact. It is recommended that exposed edges of PCB panels be reinforced with an aluminum covering to prevent these small deformities from initially forming and spreading through the circuit board.

The issue of high stress between contacting panels at the peak of deformation must also be addressed. This occurs when the system has collapsed and the internal kinetic energy from the folding mechanism has been expended.

Large amounts of energy are dissipated in both models through the kinetic energy of the panels folding. A point of investigation would be the addition of more stiff or materials that absorb the impact energy and dissipate it elastically. A stiffer material would require higher amounts of energy to deform, subtracting the amount manifesting as strain energy in the PCB or aluminum. An increase in the rotational stiffness of the bushing elements of an equivalent 1 rad/mm reduced the overall strain energy in the system by 14%.

Lastly, PUFFER's origami structure is highly restrictive to a single folding direction or "axis". Consequently, PUFFER's PCB skeleton functions poorly under loading profiles that force a torsional response. The problematic regions in these cases are the same as those discussed in the two impact cases: the top panel is prone to bending and carrying a large portion of the system's energy. A redesign of PUFFER would consider a hinge or other energy dissipating element along a torsional axis to allow for a softer system response in that mode.

The stress and strain values for the Nomex plate elements is not extracted or examined beyond ensuring that the model is functioning correctly. With the implementation of the Ogden model of hyperelasticity, stress and strain values are no longer reflective of the original isotropic elastic fabric model. Future work should include checking failure modes related to the Nomex and the Nomex-PCB bond.

6. Analysis of Alternate Origami Rigid-Flex Robotic Structures

Alternate origami structures leveraging the proposed modeling methodologies and takeaways from PUFFER's impact performance are presented in this section. The PCB and Nomex hinges use the same values as the PUFFER architecture. The proposed architectures are used to study general design principles for rigid-flex PCB robotics and do not necessarily reflect a constructible design (electronics components and mobility elements are not modeled). Two different rigid-flex PCB architectures are presented and shown in Figures 17 and 18. Included in this study is PUFFER's base architecture, for reference.

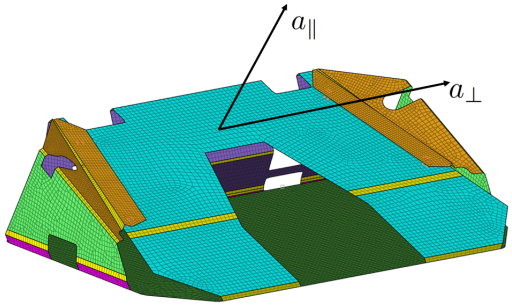

Figure 17. First presented architecture - PUFFER redesign with 11 panels and 19 joints

Figure 17 shows a reworked PUFFER architecture with two additional joints in the largest panel. The addition of the two hinges permits the rear end of the structure to collapse 28° without introducing bending into the front, which was previously problematic. Figure 18 is inspired by a classic

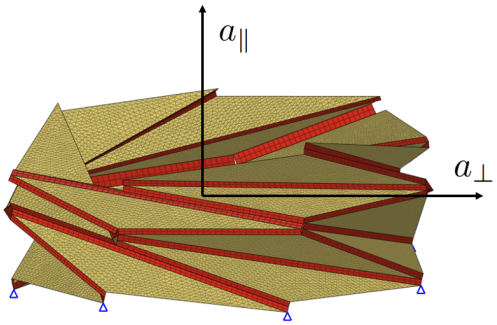

Figure 18. Second presented architecture - cylindrical helix collapsible structure with 28 panels and 36 joints

cylindrical origami structure with folding mechanisms aligning with the buckling of a cylindrical shell wall [22]. This structure was selected with a large range of motion during folding in mind. With each model, we define an axis of folding as the vector about which the origami is structured to fold without resistance.

An assessment of the two structures is performed by examining system response given an acceleration load. Define acceleration forces parallel to and perpendicular to the axis of folding as $a_{\parallel}$ and $a_{\perp}$, respectively. Let a positive $a_{\parallel}$ be in the direction of system expansion and a negative $a_{\parallel}$ be in the direction of system compression. For each model, six cases are presented with the following loads.

Table 5. Loading Conditions for Alternate Origami Rigid-Flex Robotic Structures

Load Case	$a_{\parallel}$ (g)	$a_{\perp}$ (g)
1	-50	0
2	-100	0
3	-200	0
4	0	50
5	0	100
6	-70.71	70.71

Both parallel and perpendicular components are considered in the 6th case to create a net of $100g$ acceleration loading at a 45° to the axis of folding. In addition to evaluating the structural requirements presented in Section 4, energy criteria and velocity results are also presented. This will form the basis of the more generalized rigid-flex PCB robotic design criteria.

The PUFFER impact study revealed the highly sensitive nature of long, exposed PCB segments to impact loading. For this reason, this study assumes a stiffening or encasing material will be covering the bottom (dark green) panel in the revised PUFFER architecture shown in Figure 17. The impact point is assumed to be along the base and that the stiffening elements are rigid enough to assume the rest of the structure moves relative to the base with impact accelerations given in Table 5. In a similar methodology, the bottom nodes adjacent to the hinges of the cylindrical helix structure are restrained in the U1, U2, and U3 directions to represent a rigidized area where electronics components might be protected, similar to PUFFER's aluminum base. These restraints can be seen in blue in Figure 18. A gravitational constant of 9.81 m/s^2 is applied to each model. Table 6 summarizes the results relevant to Section 4, including an additional parameter, the maximum change in volume (ΔV, mm^3).

It should be noted that the time to maximum change in volume, in either system compression or extension, is maximized when $a_{\parallel}$ is the governing condition. Consequently, the δ_T values are considerably reduced compared to other load cases. Intuitively, origami structures are the most compliant and result in the largest volume change when forced into their folded configurations. This is advantageous for the design of rigid-flex robotics - robotic structures with folding mechanisms along multiple axis will reduce the damage to the system upon impact.

Additionally, we see a large reduction in the stresses between the redesigned PUFFER and the original PUFFER architectures through the addition of the additional hinge. The once large and thin PCB panel split by a Nomex hinge in the redesign now experiences much less normal bending in all three acceleration loading directions. This reduces the need for discrete stiffening of the PCB panel and allows for the system to retain it's original low-mass characteristic.

Table 7 provides additional results from the same models. For brevity, the acceleration load direction is not supplied in the table but is identical to that referenced in Table 6. Let the subscript $\Delta Vmax$ indicate that the energy value was taken at the time of maximum change in volume. The table presents the architecture and load case number, the average deceleration of the center of gravity of the panels just before contact or the time of maximum volume change (a_{decel}), the percentage of kinetic energy in the panels dissipated at the maximum volume change ($E_{KE}^{\Delta Vmax}$), and the percentage of the total energy dissipated as strain energy in the panels at the maximum volume change ($E_{E}^{\Delta Vmax}$).

We observe that the PUFFER redesign model has a slower average deceleration than the original PUFFER architecture. Under a dynamic load, the additional hinge allows for the system to come to a slower stop, reducing some of the stresses that manifest in the panels. Along the same lines, the cylindrical helix is highly compliant and has an even lower average deceleration value. A final observation is the cylindrical helix dissipates much higher amounts of kinetic energy than the other architectures through the complex folding mechanism.

7. Design Recommendations of Rigid-Flex PCB Robotic Structures

This paper presented structural considerations that must be taken when designing and performing modeling of a rigid-flex PCB system and several other origami architectures for reference. From the presented studies, the following design recommendations are given.

1 - Sensitive electronic components should not be mounted to exterior-facing PCB panels

2 - Large electronic components should not be mounted to panels that may experience direct impact force causing discrete bending strain and solder failure

3 - Long, slender PCB panels with a length more than 30x the thickness should be stiffened

Table 6. Relevant Model Results for Structural Design

Architecture	Load Case	Acceleration load dir.	δ_T (mm)	Maximum stress (MPa)	Time to max. ΔV (ms)
PUFFER	1	$a_{\parallel}$	7.212	14.49	13.69
PUFFER	2	$a_{\parallel}$	16.924	28.97	12.49
PUFFER	3	$a_{\parallel}$	18.475	57.94	11.79
PUFFER	4	$a_{\perp}$	0.625	8.169	1.99
PUFFER	5	$a_{\perp}$	1.630	16.34	1.84
PUFFER	6	$a_{\parallel}$ and $a_{\perp}$	8.124	28.63	12.89
PUFFER redesign	1	$a_{\parallel}$	3.734	5.14	15.15
PUFFER redesign	2	$a_{\parallel}$	7.367	10.30	13.15
PUFFER redesign	3	$a_{\parallel}$	14.340	20.60	11.65
PUFFER redesign	4	$a_{\perp}$	0.419	6.34	1.65
PUFFER redesign	5	$a_{\perp}$	0.647	10.54	1.14
PUFFER redesign	6	$a_{\parallel}$ and $a_{\perp}$	6.882	18.69	13.05
Cylindrical helix	1	$a_{\parallel}$	0.324	6.42	18.48
Cylindrical helix	2	$a_{\parallel}$	0.388	8.87	15.65
Cylindrical helix	3	$a_{\parallel}$	0.647	11.58	11.14
Cylindrical helix	4	$a_{\perp}$	1.245	16.55	1.41
Cylindrical helix	5	$a_{\perp}$	1.877	18.45	0.98
Cylindrical helix	6	$a_{\parallel}$ and $a_{\perp}$	0.972	9.83	15.98

Table 7. Dynamic Response and Energy Dissipation in Various Rigid-Flex PCB Architectures

Architecture	Load Case	a_{decel} (mm/ms^2)	$E_{KE}^{\Delta V max}$ dissipated (%)	$E_{E}^{\Delta V max}$ (%)
PUFFER	1	1.88	54.2	14.9
PUFFER	2	2.94	47.8	18.6
PUFFER	3	6.90	22.4	40.4
PUFFER	4	12.01	4.6	56.5
PUFFER	5	28.47	3.6	78.4
PUFFER	6	11.54	39.1	80.0
PUFFER redesign	1	0.95	78.7	28.9
PUFFER redesign	2	1.90	52.4	47.0
PUFFER redesign	3	4.43	31.7	59.5
PUFFER redesign	4	2.70	62.4	91.2
PUFFER redesign	5	7.35	5.7	65.4
PUFFER redesign	6	2.27	44.5	90.2
Cylindrical helix	1	1.55	44.8	15.5
Cylindrical helix	2	2.08	35.9	21.6
Cylindrical helix	3	2.17	34.7	55.8
Cylindrical helix	4	4.65	39.9	68.9
Cylindrical helix	5	5.11	38.4	80.5
Cylindrical helix	6	2.86	34.6	74.3

4 - Different types of hinges with varying degrees of rotational stiffness should be examined based on demand

5 - Exposed cut edges of PCB should be sealed or reinforced

6 - A more massive and stiff portion should be added to a rigid-flex PCB system (in PUFFER, the aluminum base serves this purpose) to prevent constant interpanel contact

7 - Fasteners should be kept planar

8 - Holes in PCB sections for wheels or other attached parts should be a satisfactory distance into the panel to prevent tearout

9 - The origami structure should be such that torsional loads have a method of dissipation other than damage to the system

10 - Origami design should have more than one axis of compliance, if possible

ACKNOWLEDGMENTS

This work is supported by the NASA South Carolina Space Grant Consortium with grant number 521383-RP-CM002 (REAP). The research was carried out with the Jet Propulsion Laboratory, California Institute of Technology, under a contract with the National Aeronautics and Space Administration (80NM0018D0004).

REFERENCES

[1] Balkcom, D. J., & Mason, M. T. (2004). Introducing robotic origami folding. *IEEE International Conference on Robotics and Automation, 2004. Proceedings. ICRA '04. 2004.* https://doi.org/10.1109/robot.2004.1308754

[2] Balkcom, D. J., & Mason, M. T. (2008). Robotic Origami Folding. *The International Journal of Robotics Research, 27(5), 613–627.* https://doi.org/10.1177/0278364908090235

[3] Karras, J. T., Fuller, C. L., Carpenter, K. C., Buscicchio, A., McKeeby, D., Norman, C. J., Parcheta, C. E., Davydychev, I., & Fearing, R. S. (2017). Pop-up Mars rover with textile-enhanced rigid-flex PCB body. *2017 IEEE International Conference on Robotics and Automation (ICRA).* https://doi.org/10.1109/icra.2017.7989642

[4] DuPont, Nomex Technical Guide. Technical report, 2019.

[5] Steinberg, D. S. (2000). *Vibration Analysis for electronic equipment*. Wiley Interscience Imprint.

[6] Gu Jie, Lim, C. T., & Tay, A. A. O. (n.d.). Modeling of solder joint failure due to PCB bending during drop impact. *Proceedings of 6th Electronics Packaging Technology Conference (EPTC 2004) (IEEE Cat. No.04EX971).* https://doi.org/10.1109/eptc.2004.1396694

[7] Kovtun, I. I., Boiko, J. M., & Petrashchuk, S. A. (2021). Mathematical model for Dynamic Force analysis of printed circuit boards. *Journal of Physics: Conference Series, 1921*, 012120. https://doi.org/10.1088/1742-6596/1921/1/012120

[8] Mercado, L. L., Phillips, B., Sahasrabudhe, S., Sedillo, J. P., Bray, D., Monroe, E., Lee, K. J., & Lo, G. (2006). Handheld use condition-based bend test development. *IEEE Transactions on Advanced Packaging, 29(2)*, 240–249. https://doi.org/10.1109/tadvp.2006.871201

[9] Arabi, F., Gracia, A., Deletage, J.-Y., & Fremont, H. (2018). Vibration test and simulation of printed circuit board. *2018 19th International Conference on Thermal, Mechanical and Multi-Physics Simulation and Experiments in Microelectronics and Microsystems (EuroSimE).* https://doi.org/10.1109/eurosime.2018.8369909

[10] Bell, J., Redmond, L., Carpenter, K., & de la Croix, J.-P. (2020). Dynamic characterization of a pop-up folding flat explorer robot (PUFFER) for planetary exploration. *Topics in Modal Analysis & Testing, Volume 8*, 383–391. https://doi.org/10.1007/978-3-030-47717-2-39

[11] Abaqus 6.11. Abaqus Keywords Reference Manual. 2020.

[12] Žmindák, M., Pelagić, Z., Pastorek, P., Močilan, M., & Vybošťok, M. (2016). Finite element modelling of high velocity impact on plate structures. *Procedia Engineering*, 136, 162–168. https://doi.org/10.1016/j.proeng.2016.01.191

[13] Smojver, I., & Ivančević, D. (2011). Bird strike damage analysis in aircraft structures using Abaqus/explicit and coupled Eulerian Lagrangian approach. *Composites Science and Technology*, 71(4), 489–498. https://doi.org/10.1016/j.compscitech.2010.12.024

[14] Buitrago, B. L., Santiuste, C., Sánchez-Sáez, S., Barbero, E., & Navarro, C. (2010). Modelling of composite sandwich structures with honeycomb core subjected to high-velocity impact. *Composite Structures*, 92(9), 2090–2096. https://doi.org/10.1016/j.compstruct.2009.10.013

[15] Ventsel, E. (2001). *Thin plates and shells: Theory, analysis, and applications*. Marcel Dekker.

[16] Boresi, A. P., & Schmidt, R. J. (2018). *Advanced Mechanics of Materials.* Wiley.

[17] T. Irvine, "Extending Steinberg 's Fatigue Analysis of Electronics Equipment Methodology to a Full Relative Displacement vs. Cycles Curve," pp. 1–29, 2013.

[18] Vianco, P., Understanding the Reliability of Solder Joints used in Advanced Structural and Electronics Applications: Part 1- Filler Metal Properties and the Soldering Process. *Welding Journal Supplement*, 2017. 96: p. 39-52s.

[19] Vianco, P., Understanding the Reliability of Solder Joints Used in Advanced Structural and Electronics Applications: Part 2-Reliability Performance. *Welding Journal Supplement*, 2017. 96: p. 83-94.

[20] Ross, R. G. (1991). A systems approach to solder joint fatigue in spacecraft electronic packaging. *Journal of Electronic Packaging*, 113(2), 121–128. https://doi.org/10.1115/1.2905377

[21] Abaqus 6.11. Abaqus Theory Manual. 2020.

[22] Jianguo, C., Xiaowei, D., Ya, Z., Jian, F., & Yongming, T. (2015). Bistable behavior of the cylindrical origami structure with Kresling pattern. *Journal of Mechanical Design,* 137(6). https://doi.org/10.1115/1.4030158

BIOGRAPHY

John Bell *received his BS in mathematics from North Greenville University, MS in structural engineering from Clemson University, and is pursuing a PhD in structural engineering from Clemson University. His area of research is structural dynamics focused on mobile robots for space exploration applications.*

Laura Redmond *is an Assistant Professor of Civil and Mechanical Engineering at Clemson University and the head of the Clemson Advanced Structures Laboratory. She earned the Ph.D. in Civil Engineering from Georgia Tech in 2015. Prior to joining Clemson in 2018, she was a Structural Engineer with the NASA Jet Propulsion Laboratory, focusing on advanced finite element simulations, rigid body dynamics models, and the development of test programs for model validation and requirements verification. Dr. Redmond's research interests include advanced structural and dynamics simulations, formal model verification, and model validation by test.*

Kalind Carpenter *is a Robotics Engineer in the Robotic Vehicles and Manipulators Group (347B). The lab he works in focuses on rapid technology development and end effectors specifically tailored to gripping and rough surface mobility. He has received his MS in mechanical engineering from CSULA. Current work includes (Co-I) on PUFFER, Ocean Worlds Mobility Study, micro ground vehicles tasks, designing wall climbing robots that utilize microspines, and electrostatic and Gecko adhesive to climb vertical surfaces.*

Jean-Pierre de la Croix *is a Robotics Systems Engineer in the Robotic Systems Estimation, Decision, and Control group. He joined JPL after completing a Ph.D. in Electrical and Computer Engineering at the Georgia Institute of Technology in 2015. His research focused on new control techniques for large-scale robotic systems, such that humans can easily and effectively interact with these complex systems. At JPL, he continues to work on multi-agent robotics for new and challenging applications.*